Research Square

Preprints are preliminary reports that have not undergone peer review. They should not be considered conclusive, used to inform clinical practice, or referenced by the media as validated information.

# Application Study of a water conducting fracture zone height prediction model based on bp neural network optimized by genetic algorithme—Shendong mining area

**Chunwei Ling**

chunweiling@163.com

Inner Mongolia Research Institute, China University of Mining and Technology (Beijing)

**Yixin Zhao**

China university of mining and technology

**Bao Cao**

China university of mining and technology

**Sen Gao**

China university of mining and technology

**Zhenyu Tai**

Inner Mongolia Research Institute, China University of Mining and Technology (Beijing)

---

**Article**

**Keywords:** Height of WCFZ, Correlation analysis, Genetic algorithm, BP neural network, GA-BP network model

**Posted Date:** September 24th, 2026

**DOI:** https://doi.org/10.21203/rs.3.rs-10953860/v1

**License:** This work is licensed under a Creative Commons Attribution 4.0 International License. Read Full License

**Additional Declarations:** No competing interests reported.

---

**Version of Record:** A version of this preprint was published at Scientific Reports on October 13th, 2026. See the published version at https://doi.org/10.1038/s41598-026-75952-9.

# Application Study of a water conducting fracture zone height prediction model based on bp neural network optimized by genetic algorithme—Shendong mining area

Chunwei Ling[1,2], Yixin Zhao[1,3], Bao Cao[1,3], Sen Gao[1,3], Zhenyu Tai[1,3]

1 Inner Mongolia Research Institute, China University of Mining and Technology (Beijing), Ordos, 017010, China

2 China Coal Research Institute, Beijing 100013, China

3 School of Energy and Mining Engineering, China University of Mining and Technology (Beijing), Beijing 100083, China

*Corresponding Authors: Chunwei Ling E-mail address: chunweiling@163.com

**Abstract:** It is important to accurately predict the height of the water conducting fracture zone (WCFZ) for the production safety of coal mines and ecological environmental protection. Through the field measurement data of WCFZ at working face in Shendong and neighboring mines. The correlation degree between the working face length, mining height, mining depth, coal seam dip angle, mining speed, hard rock proportionality coefficient and the height of WCFZ was analyzed by using gray relationship analysis theory. The BP neural network model optimized by genetic algorithm was trained, and the predicted WCFZ values of empirical formula, GA-BP and BP neural network model were compared with the actual measured values of WCFZ in the mine area. The comparison analysis showed that the GA-BP neural network model had the smallest error of 7.78% in the prediction value. Therefore, the GA-BP neural network model has sufficient prediction accuracy and generalizability and can be applied to study the WCFZ in the Shendong mine area.

**Keywords:** Height of WCFZ, Correlation analysis, Genetic algorithm, BP neural network, GA-BP network model

## 1. Introduction

The exploration of coal resources in northwest China has led to more serious ecological problems in mining areas with fragile ecological and geological environments [1–3]. The technology and equipment in China was improving constantly to keep up with the increasing demand for mining coal resources. However, because of the occurrence characteristics of coal resources of great reserves, high quality coal, shallow depth of burial, simple geological structure, and relatively stable coal seam, the widely adopted high-intensity mining in Shendong mining area has led to a drop in the water table through water conducting fractures, further worsening the fragile ecological environment of the arid and semi-arid areas [4,5]. In order to achieve the balance and harmony between coal resources mining and water resources carrying capacity, it is necessary to study the theoretical basis and key parameters of the height of water conducting fractured zone (WCFZ), which was equal to the vertical distance between the upper boundary of WCFZ and the coal seam.

The main methods of calculating the WCFZ were based on empirical formulas, numerical simulations, physical simulations and field measurements. According to the movements and fractures of overlying strata caused by underground mining, three different zones can be continuously divided above the goaf as the caving zone, fractured zone and subsidence zone [4,6,7]. Based on the mine field measurement

data, an empirical formula was established. By calculating and analyzing the height of the caving zone and height of the WCFZ in the western mine, it is concluded that the damage height of the overburden was related to the overburden property. The height of the caving zone was 2-8 times the mining height and the height of WCFZ was 30-50 times the mining height [4,5,8]. If the vertical distance between the location of the main key stratum and the location of the coal seam was small, the height of WCFZ calculated by physical simulation analysis was greater than the height value calculated by the empirical formula [6,9,10]. The empirical formula method can estimate the height of WCFZ quickly, however, due to the increase of working face size, it is no longer applicable to calculate the height of WCFZ [4,5,11,12].

By analyzing different working face thickness and mining depth through numerical simulation and similar simulation, the height of WCFZ and the thickness of protective layer can be calculated [5,12–15]. However, the results of physical simulation have difference from the measured results because of the scale effect, which resulted from the restricted size of the physical model. According to the numerical simulation and empirical formula, the WCFZ increases with increasing working face length and mining height [5,14]. In all numerical simulation methods, the discrete element method is usually used to analyze fracture characteristics, such as mining-induced fractures, rather than the continuum element method [7,16,17]. But the analysis of WCFZ need a quite large model, which will spend a lot of time with its construction and calculation. Besides, the local refinement is often necessary for

simulating the morphological characteristics of fractures.

The support vector regression (SVR) method is used to predict the WCFZ based on the field measurement data to improve the accuracy and stability of the prediction [18]. Multiple regression analysis and neural network models can also accurately predict the height of WCFZ [19–26]. As a single factor was considered in the regression analysis, it will lead to inaccurate prediction. Therefore, a massive amount of sample data was required to improve the accuracy of prediction.

In this paper, the measured WCFZ at the working face in Shendong mine and around were collected, and the working face size, mining depth, mining height, dip angle of coal seam, mining speed and proportion coefficient of hard rock were taken as the dominant impact factors of the height of WCFZ. The correlation between each influencing factor and the height of WCFZ was analyzed. The WCFZ height prediction model was established by training the GA-BP neural network model, which provides a reference basis for coal mining and water resource protection in the Shendong mining area.

## 2. Evolution characteristics and influencing factors height of WCFZ

### 2.1 Evolution characteristics of WCFZ

As shown in Fig. 1, due to the broken overlying rock layer after coal mining. The damage of the overburden layer can be divided into collapse zone, fracture zone and bending sinking zone. The caving zone was filled with irregularly shaped top rock, and the height of caving zone was 2~8 times mining height [4]. The overburden was

broken, collapses, and accumulates into the goaf. The broken rock mass that filling the goaf ultimately form a support zone for the overburden. The height of the overburden was limited, as the crushed rock blocks in the goaf were compacted, the overburden bends and fractures, forming a fractured zone. The bed separation zone is going to close up and be poor water-conductivity with the compaction under the influence of the overburden weight. Vertical fractures formed by shearing extend to the surface and serve as conduits for surface air and water. The subsidence zone was located between the fractured zone and the ground, where was far from the coal seam and was less affected by mining. Its internal bending movement deformation will also produce some fractures. These fractures were disconnected from each other, so that the curve subsidence zone remains consistent and complete.

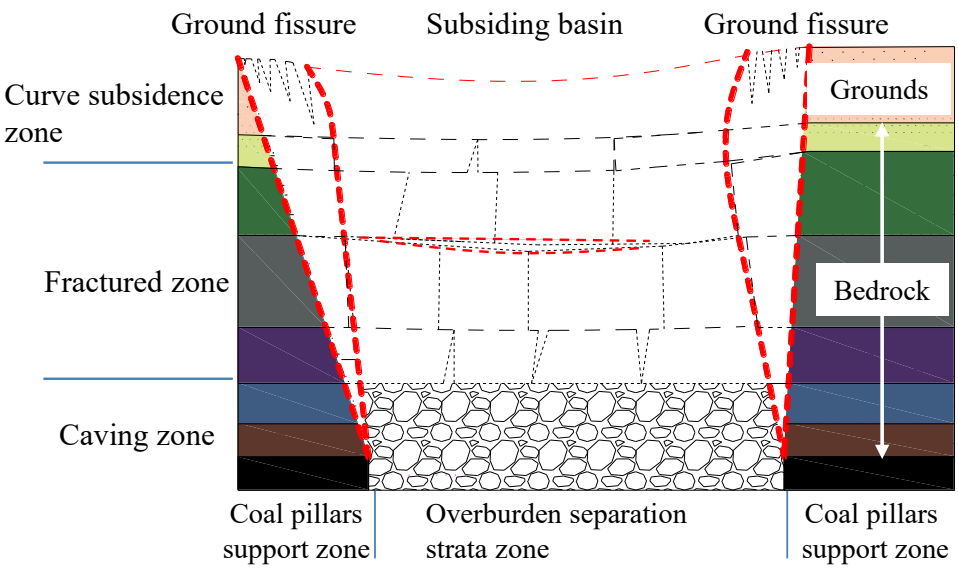


**Fig.1** Caving zone, fractured zone and curve subsidence zone of overlying strata above the goaf

### *2.2 The failure mode of "two-zone" structure*

For the high-intensity mining of the thick coal seam with shallow buried depth in Shendong mining area, the overburden rock follows the failure mode of "two-zone" structure, in which the caving zone is seriously broken with a great extension of height. There are two types of breaking mode, one is that the overburden rock from the coal seam to the ground are cut off as a whole, will result in fractures extend from the goaf to the ground and present as steps on the ground. The second mode is that the key strata breaks to form the masonry beam structure, will cause to rapidly extends of fractures upward to the ground. Ground fractures caused by the second mode are mainly tensile type [11,27].

Table 1 "Two-zone" formula for full mechanized mining

| Overlying strata type | The height of caving zone（m） | Formula 1: The height of WCFZ（m） | Formula2: The height of WCFZ（m） |
|---|---|---|---|
| Hard rock | 7M+5 | $\frac{100M}{0.15M+3.12}\pm 11.18$ | 30M+10 |
| Medium-hard rock | 6M+5 | $\frac{100M}{0.23M+6.10}\pm 10.42$ | 20M+10 |
| Weak rock | 5M+5 | $\frac{100M}{0.31M+8.81}\pm 8.21$ | 10M+10 |

Note: *M* in the table is the mining height, ranging from 3 to 10 m.

Table 1 is the empirical formula concluded by engineering technicians in Shendong mining area based on decades of mining experience [4,14]. Normally, the empirical formula method calculates the height of WCFZ of working face, however, with the high degree of comprehensive mechanization mining technology, the increase in the size of the working face, and the increase in the mining speed and other factors, this calculation method was no longer applicable to the calculation of

the WCFZ in Shendong mining area [5]. As shown in Fig. 2.

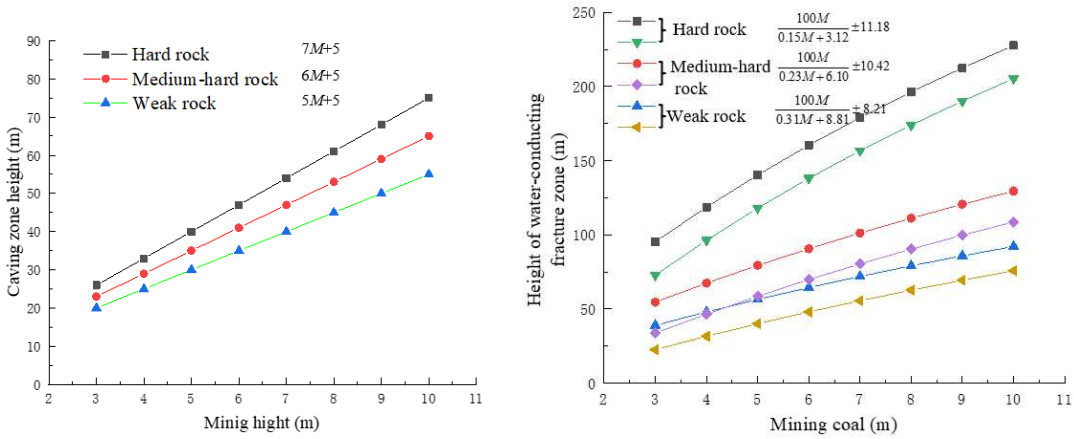


（a）The height caving zone （b）Formula 1

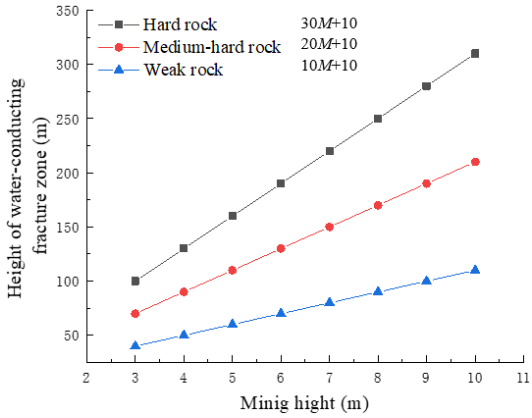


（c）Formula 2

**Fig.2** The height of the fractured zone in full mechanized mining

### *2.3 Influencing factors of the height of WCFZ*

By collecting data samples and references from various mines, influencing factors of the height of WCFZ include the coal seam depth, mining thickness, overburden property, working face size, coal seam dip angle and mining speed, as shown in Fig. 3.

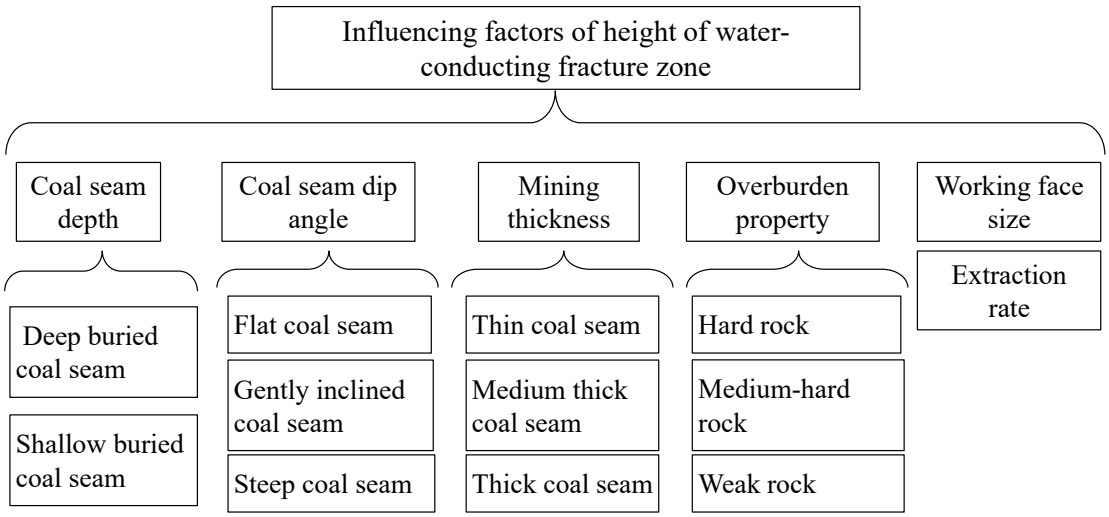


**Fig.3** Influencing factors of the height of WCFC

The coal seam storage feature of Shendong mine area were based on near horizontal coal seam and shallow buried coal seam, and the working face design width, working face length, mining height and mining speed were generally 100~400 m, 300~360 m, 1000~3000 m, 3.5~8 m, and 5~20 m/d, respectively. According to the experience of statistical law of rock mechanical strength [5], the overlying strata of the coal seam was divided into four categories as hard rock stratum, medium-hard rock stratum, weak rock stratum and extremely soft rock stratum. The main components of the hard rock formations are quartz sandstone, limestone, conglomerate, sandstone and argillaceous limestone. The main components of the medium-hard rock formations are sandy shale and shale, and soft rock mainly composed of mudstone and sandy mudstone. The main components of the weak rock formations are bauxite, weathered mudstone, clay and sandy clay.

## 3. Building GA-BP neural network training model

### *3.1 Modeling approaches*

A genetic algorithm (GA) is a search algorithm built by simulation of the genetic and evolutive processes in the biological world. GA starts with a population of all possible potential problems and selects individuals that are better suited to the environment based on method of simulates natural selection. In this process, individuals of the population evolve, and thus a new set of population is generated to adapt to the environment better [28,29], as shown in Fig. 4.

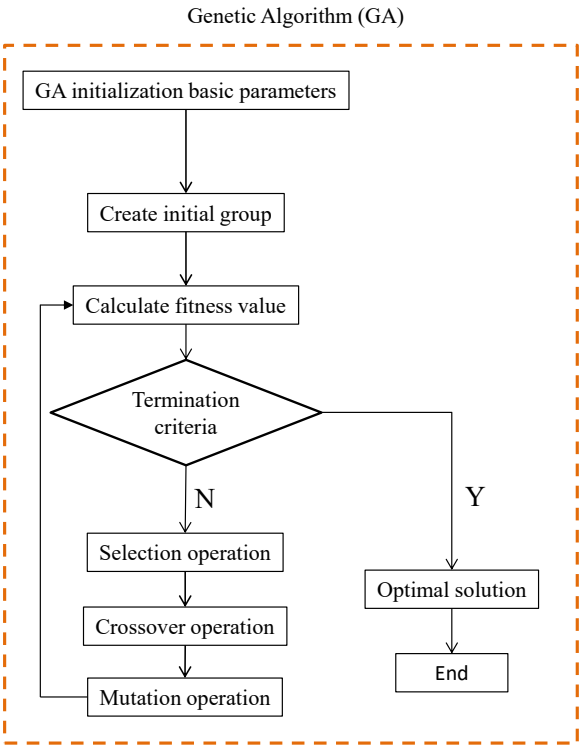


**Fig.4** Genetic algorithm flow chart

Fig. 5 shows a Back Propagation (BP) neural network topology model with WCFZ height, consisting of three parts, including input, hidden and output layers, each of which can be one or more layers [30,31]. During the training of the BP neural

network model, it can be transmitted forward and backward. Forward transmission refers to the transmission of the input sample data from the input layer to the hidden layer, which is processed by the hidden layer, and then passed to the output layer. The state of the neurons in each layer affects only one layer, and no accurate output information is obtained in the output layer, the error information was back at the same time along the same path, and the weapons of the connections of each neuron are also modified at the same time. After continuous iteration, the final error signal reaches the allowable range.

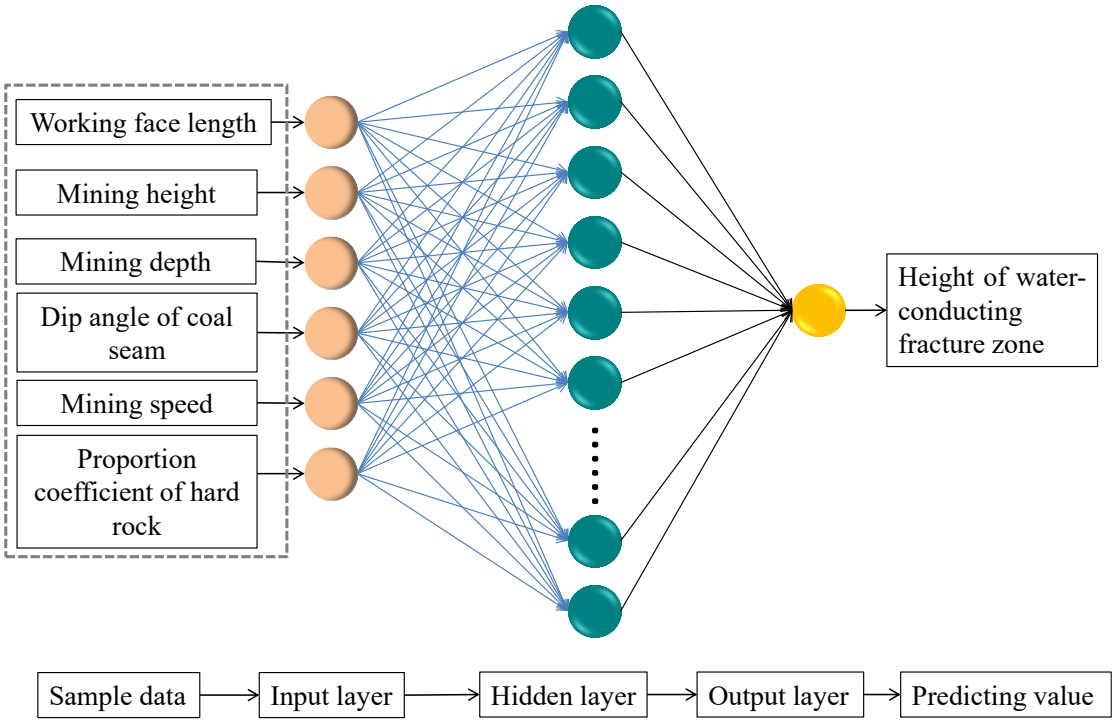


**Fig.5** Topological structure model of the BP neural network for the height of WCFZ

GA-BP network model was genetic algorithm to optimize BP neural network [24]. Obtain the optimal initial weight and threshold of the BP network through the global search ability of genetic algorithm, and use the optimal initial weight and threshold obtained by the search algorithm as the initial weight and threshold of the

BP neural network, and then train it to avoid falling into local minimum values. The weights of the BP neural network improved by genetic algorithm were not randomly generated, but are obtained by the genetic algorithm search module.

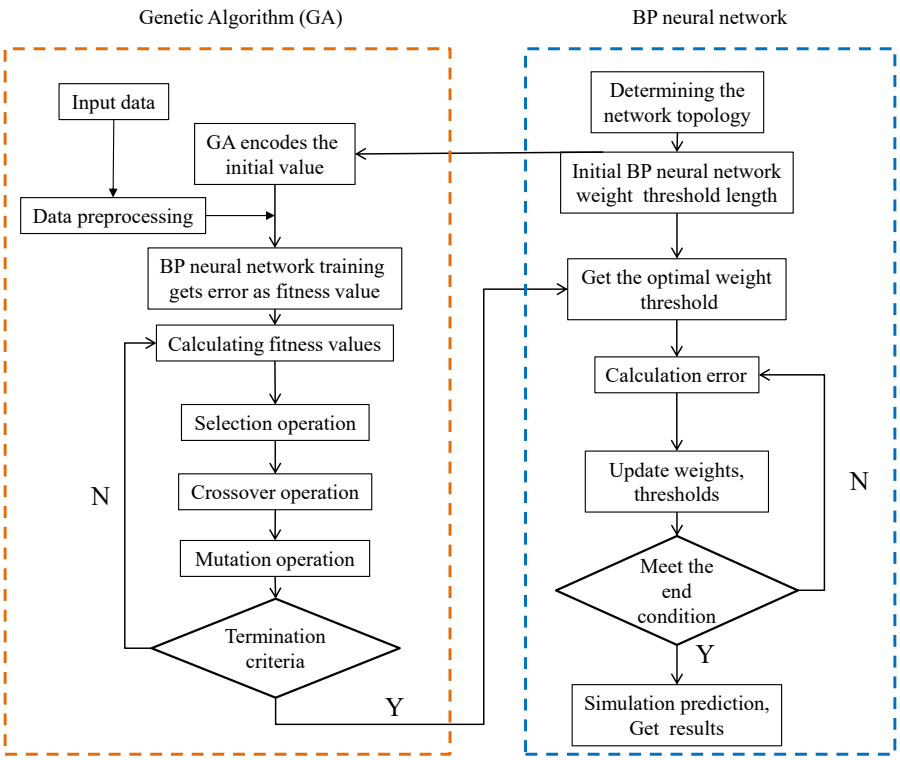


**Fig.6** GA-BP neural network algorithm flow chart

The optimal number of hidden layer nodes in the neural network structure was determined by optimizing the BP neural network with genetic algorithm. The GA-BP neural network algorithm flow chart was shown in Fig. 6. The steps are as follows: (1) Set the initial population of hidden layer nodes to GA, construct a BP network topology, and then use GA to change the initial weights and thresholds in the neural network structure to optimize the fitting function, (2) Starting from any initial population, random selection, crossover, and mutation operations were carried out, after multiple iterations, the output layer of the BP neural network reaches the

maximum number of evolutions, (3) Finally, the topology of the BP neural network was determined by the best individual in the population.

### *3.2 Obtain parameter samples and pretreatment*

Training the height of WCFZ prediction model of Shendong mine area by the established GA-BP network model, factors affecting WCFZ height were quantitatively selected, such as working face length ($L$), mining height ($M$), mining depth ($H_d$), dip angle of coal seam ($D$), mining speed ($V$) and hard rock proportion coefficient ($b$). As listed in Table 2, the measured data of 20 working faces in Shendong and its surrounding mining areas were selected as training and test samples of the GA-BP network model.

Table 2 Sample data of the height of WCFZ

| No. | Coal mine | $L$ (m) | $M$ (m) | $H_d$ (m) | $D$ (°) | $V$（m/d） | $b$ | The height of WCFZ (m) |
|---|---|---|---|---|---|---|---|---|
| 1 | Bulianta 32301 | 301 | 5.7 | 212 | 3~7 | 13 | 0.56 | 67.3 |
| 2 | Bulianta 12406 | 300 | 4.8 | 200 | 5.38~16 | 12 | 0.66 | 41.39 |
| 3 | Bulianta 31401 | 300 | 4.2 | 255 | 3~7 | 7.8 | 0.71 | 70.1 |
| 4 | Bulianta 22307 | 301 | 6.8 | 92 | 1.76~8 | 8 | 0.63 | 75.6 |
| 5 | Bulianta 52307 | 301 | 6.7 | 190 | 0~2.2 | 10.8 | 0.49 | 52.6 |
| 6 | Bulianta 12610 | 200 | 5.0 | 135.0 | 1~3 | 8.2 | 0.33 | 50 |
| 7 | Bulianta 1203 | 150 | 6 | 49.0 | 5 | 7.8 | 0.44 | 45.0 |
| 8 | Halagou 22407 | 284 | 5.3 | 130 | 1~11 | 15 | 0.86 | 73.6 |
| 9 | Halagou 02201 | 210 | 6 | 124 | 0~3 | 7.5 | 0.43 | 56 |
| 10 | Zhangjiamao 14202 | 295 | 4 | 180 | 1~3 | 8 | 0.31 | 72 |
| 11 | Zhangjiamao 15201 | 260 | 6.2 | 133 | 1~3 | 10 | 0.43 | 89.6 |
| 12 | Hanjiawan 2304 | 268 | 4.1 | 135 | 1.8~7.6 | 9.0 | 0.68 | 56.3 |
| 13 | Lijiahao 31110 | 240 | 4 | 343.5 | 1~3 | 9.5 | 0.5 | 85.3 |
| 14 | Yuyang 23041 | 200 | 3.5 | 188 | 0.28 | 6.7 | 0.51 | 86 |
| 15 | Shangwan 51101 | 240 | 5.5 | 146 | 2.5~9 | 8.0 | 0.61 | 50.63 |
| 16 | Huojitu 12205 | 235 | 3.5 | 85 | 1~3 | 12 | 0.4 | 75 |
| 17 | Buertai 23101 | 300 | 3.0 | 327 | 3 | 6.5 | 0.59 | 55.5 |
| 18 | Wulanmulun 2207 | 284.3 | 5.4 | 131 | 1 | 15 | 0.47 | 67.2 |

| | | | | | | | | |
|---|---|---|---|---|---|---|---|---|
| 19 | Cuncaota 43115 | 360 | 2.3 | 101.6 | 1~3 | 6.1 | 0.36 | 34.0 |
| 20 | Shigetai 12105 | 300 | 2.5 | 85.5 | 1~3 | 9.1 | 0.81 | 58 |

MATLAB program was written for training genetic optimization BP neural network simulation training. Values of samples numbered 1 to 14 in Table 2 were used as learning sample data, and that numbered 15 to 20 were used as test sample data. The neural network convergence was accelerated and the training time was reduced to unify the units, so that the unreasonable result caused by the difference in data range were reduced. Therefore, before training the sample parameters, the sample data was normalized to map the output in the interval [0,1]. Conversely, the sample training result data needs to be anti-normalized, so that the data after calculation is the real result of the sample data. The normalization and anti-normalization formula are shown as Eq.1 and Eq. 2, respectively:

$$X_n = \frac{X - X_{\min}}{X_{\max} - X_{\min}} \tag{1}$$

where, $X_n$ is the nth normalized data of each parameter, $X_{max}$ and $X_{min}$ are the maximum and minimum values in each data set.

$$Y = Y_n (Y_{\max} - Y_{\min}) + Y_{\min} \tag{2}$$

where, $Y$ is the data after anti-normalization, $Y_n$ is the original value of training results, $Y_{max}$ and $Y_{min}$ are the original maximum and minimum values in each training result data set.

### *3.3 GA-BP model test training*

The GA-BP network model was trained to finally obtain the height prediction

model of WCFZ in the Shendong mine area. In this paper, a small amount of data were collected from experimental samples in Shendong and its surrounding mining areas, so it was feasible to choose a three-layer BP neural network to process the sample data.

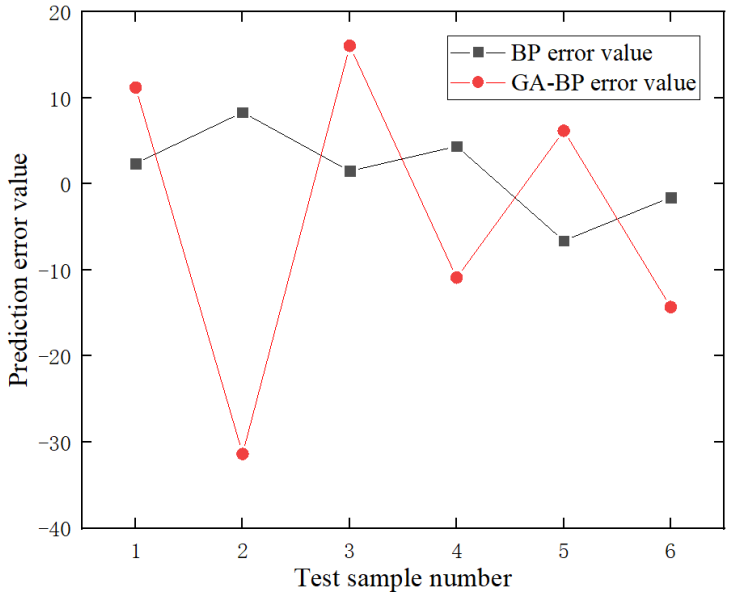


**Fig.7** The error of the predicted value using the BP and GA-BP neural network

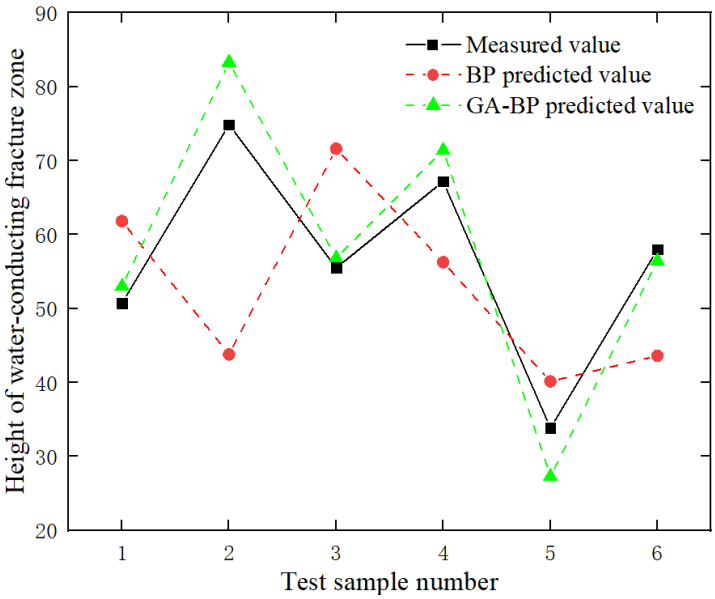


**Fig.8** Actual value and predicted value of the BP and the GA-BP neural network

As shown in Fig. 7 and Fig. 8, the prediction values after training based on the BP network model was fluctuating and unstable, with prediction error deviation

values between [-30, 18], while the prediction error deviation values after training based on the GA-BP network model was between [-10, 10], with small fluctuation and stable predicted value. By comparing the differences between the truth value and predicted value, the prediction error deviation of the GA-BP network model was [-8, 8], the fluctuation of the error deviation was smaller, and the predicted value was more stable. The results indicate that GA-BP network training model was more stable and reliable than the BP network model.

### *3.4 Validation of GA-BP network model*

In this paper, the measured data of 20 mining working faces was collected in Shendong and its surrounding mining area. The sample data was normalized, and then the GA-BP network was trained. The first 14 groups of sample data numbered from 1 to 14 were used as the training sample values, and the last 6 groups numbered from 14 to 20 were used as test values of prediction model.

The correlation coefficient (R) of the test data set samples is as follows:

$$R = \frac{Cov(x, y)}{\sqrt{Var(x)} + \sqrt{Var(y)}} \tag{3}$$

where $x$ is the expected output of the height of WCFZ, $y$ is the predicted output of the height of WCFZ, *Cover (x, y)* is the covariance of $x$ and $y$, $\sqrt{Var(x)}$ is the variance of $x$, and $\sqrt{Var(y)}$ is the variance of $y$.

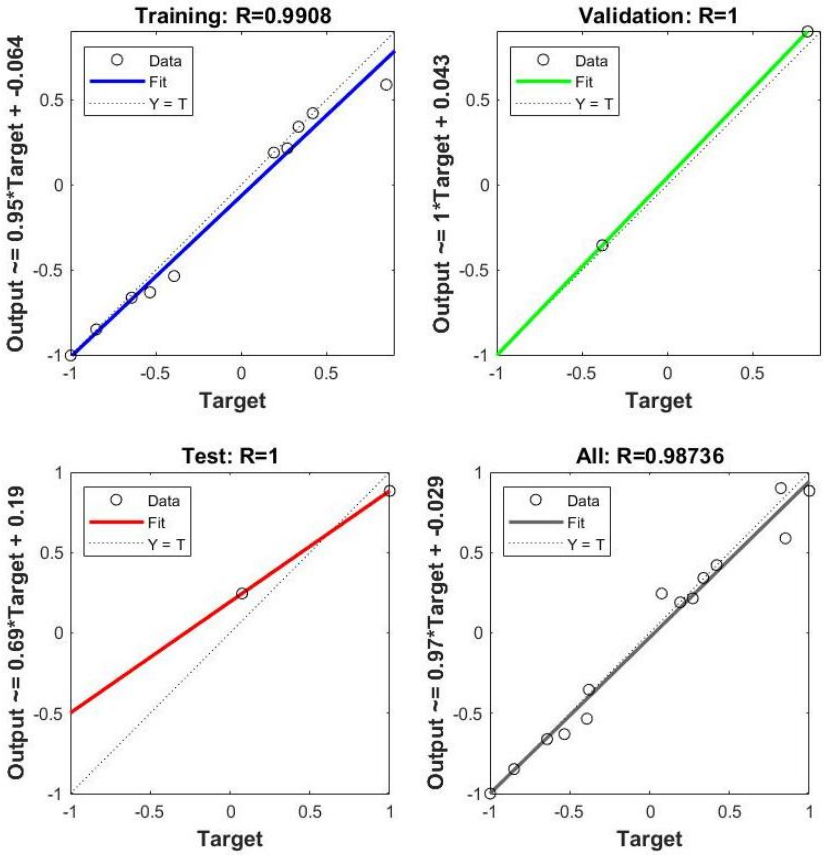


**Fig.9** Regression analysis diagram of the GA-BP neural network model

The regression analysis graph of the GA-BP neural network model was shown in Fig. 9. The training R regression value of this model was 0.9908, the validation R regression value was 1, and the test R regression value was 1. Therefore, the prediction accuracy of the trained GA-BP network model was capable of meeting the requirements of the height of WCFZ prediction. As shown in Fig. 10, the trained GA-BP neural network was retained as the "GA-BP prediction model for the height of WCFZ in Shendong mining area".

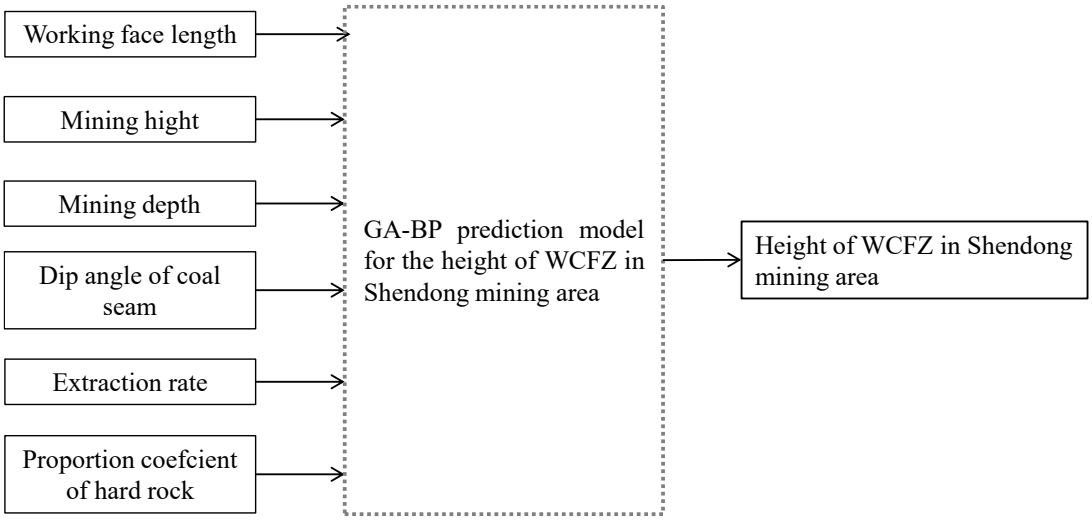


**Fig.10** GA-BP prediction model for the height of WCFZ in Shendong mining area

The BP network model had a mean absolute error of 14.9984, a mean squared error of 286.7464, a mean square root error of 16.9336, and a mean absolute percentage error of 25.35%. In comparison, the mean absolute error, mean squared error, mean square root error and mean absolute percentage error of the GA-BP network model were 4.0965, 23.4041, 4.8378 and 7.8223%, respectively. Based on the GA-BP network training model, 6 sets of test data were tested. The measured values, the predicted values of BP network model and the predicted values of GA-BP network model are listed in Table 3. The GA-BP network model was verified to have accurate prediction accuracy for the WCFZ height in Shendong mine area by the sample data.

Table 3 Error comparison between the BP and GA-BP neural network

| Prediction model | Mean absolute error | Mean square error | Root mean square error | Average absolute percentage error |
|---|---|---|---|---|
| BP neural network | 14.9984 | 286.7464 | 16.9336 | 25.35% |
| GA-BP neural network | 4.0965 | 23.4041 | 4.8378 | 7.8223 % |

# 4 Engineering verificaiton

## *4.1 The overview in the observation area*

The observation area of the height of WCFZ is located near the cutting hole of the working face No. 12304 in Shangwan coal mine with the advancing length and width of 4927.58 m and 256.8 m, respectively. The coal seam No. 12 is mined with a mining height of 3.6 m. The fully-mechanized coal winning technology is adopted, and the roof collapse naturally after coal extraction. The thickness of the overlying loose layer above the observation area is about 6~10 m, mainly loose yellowish medium-grained aeolian sand. The thickness of the coal seam was about 5 m, and the buried depth is about 300 m. The lithology of the overburden rock of the roof is mainly fine-grained sandstone, coarse sandstone and siltstone. To obtain the maximum height of WCFZ, two boreholes were arranged for the comprehensive observation method consisting of drilling flushing fluid consumption method and color drilling imaging observation method. According to the distribution characteristics of WCFZ, the biggest height of WCFZ appears near the goaf, cutting hole and stoping line. Under the medium-hard roof condition, the best observation time of the WCFZ is generally 1~2 months after mining. If the observation is too early, the WCFZ is not sufficiently developed to obtain a true maximum height. But if the observation is too late, some fractures would have been compacted and closed. Therefore, in order to observe the maximum development height of WCFZ, the positions of SW-1 and SW-2 observation holes were selected to be located at 30 m

and 127 m from the coal conveying roadway, as well as 130 meters from the open pit of Working Face 12304, as shown in Figure 11.Therefore, in order to observe the maximum development height of the WCFZ, locations of the observation boreholes were selected at 30 m and 127 m away to the transportation lane, and 130 m away from the starting cut of the working face No. 12304, as shown in Fig. 11.

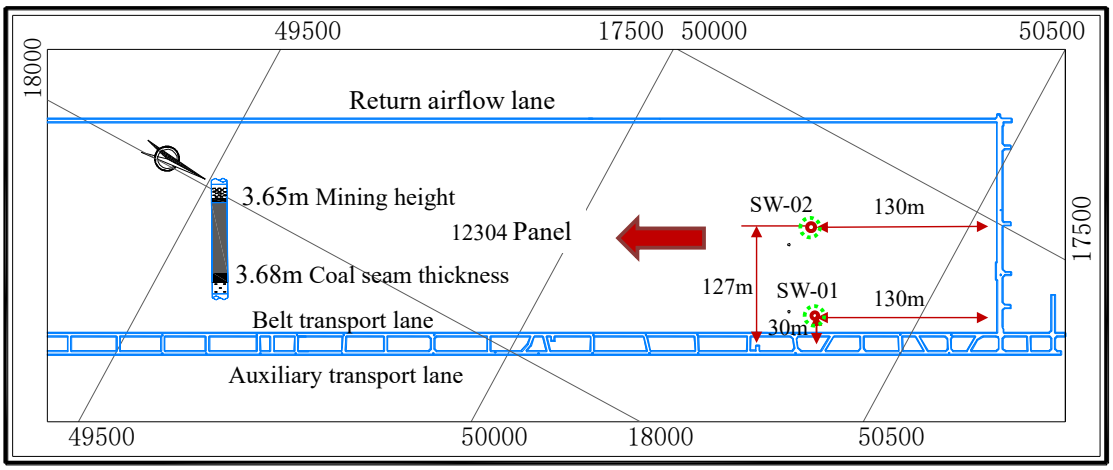


**Fig.11** 12304 The observation drilling layout of the working face No. 12304

### *4.2 Analysis of observation results*

In the process of drilling, the water level was observed before and after each drill, and the curve of the change of the water level with the drilling depth was drawn based on the obtained water level value in the borehole SW-01 before drilling, as shown in Fig. 12. The curve analysis showed that within the drilling range of 0~166.3 m, the water level in the borehole SW-01 was relatively high with a small fluctuation range. The fracture loss of the water level was less within the drilling depth of 35 m, which can be considered as a normal consumption of drilling. There was a large, rapid water consumption from 171.2 m to 169 m within the drilling depth of 66.3~171.2 m,

indicating that the fractures were relatively developed in this area. Within the drilling depth of 171~235 m, the water level rose to 169.8 m after plugging, and gradually dropped to 149.6 m in the later drilling process. When the depth of the borehole SW-01 was 240 m, the water level rapidly dropped to 235 m, indicating that fractures were obviously enlarged and the leakage of flushing fluid was intensified. When drilling down again, the water level dropped rapidly after lifting the drill. The water level was measured before running down again to show that the water in the hole has basically been completely lost.

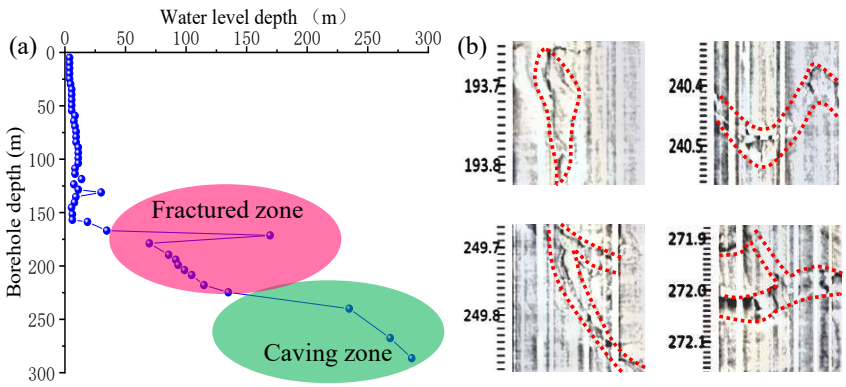


**Fig.12** Observation results of SW-01: (a) curve of the water level changing with the depth of the borehole, (b) color drilling images from the borehole

According to the result of the color drilling imaging observation, the change of flushing fluid consumption and the change of water level during drilling, the top position of the fracture zone in drill hole SW-01 was 240 m, and the fracture zone at 271.9 m was the top position of the caving zone, the location of the roof was 295.4 m. The height of fractured zone can be calculated according to Eq. 4 below:

$$H_{lie}=H-h_{lie}-W \tag{4}$$

$$H_{lie}=H-h_{k}-W \tag{5}$$

where $H_{lie}$ and $H_k$ are the maximum height of WCFZ and caving zone, respectively, in m, $H$ is the vertical depth from roof to orifice in m, $h_{lie}$ is the distance between the drilling hole position perpendicular to the top of the fracture zone, $h_k$ is the distance between the top of the collapse zone and the vertical depth of the borehole opening, $W$ is 0.2 times mining height.

Therefore, using Eq. 4 and 5, it was calculated that the height of WCFZ and the height of caving zone were 55.72 m and 24.22 m.

Fig. 13 shows the curve of the water level in the borehole SW-02 as a function of the drilling depth. At 113.56 m drill hole location, the water level in hole SW-02 dropped from 31.47 m to 100.3 m and the fracture was more developed. At the 172.23 m drill hole location, the water level dropped from 33.6 m to 50.0 m and the fracture was developed at 170.20 m. At the 244.08 m drill hole location, the water level in the hole dropped from 46.42 m to 104.0 m, and eventually stabilize at about 100 m.

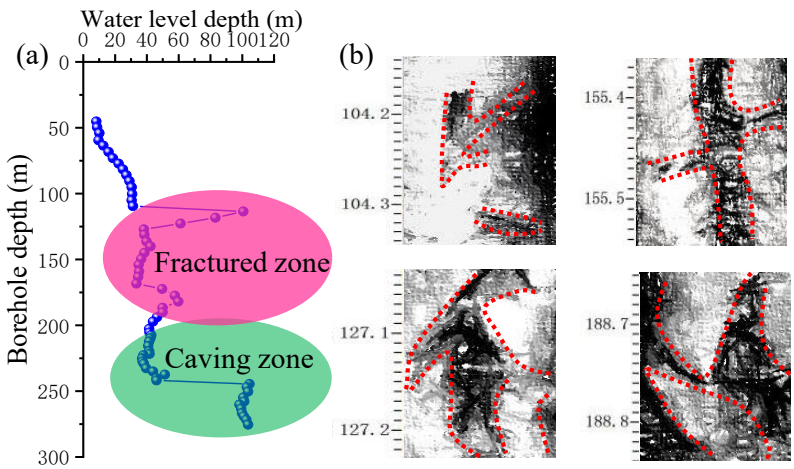


**Fig.13** Observation results of borehole SW-02: (a) the curve of the water level changing with the drilling depth, (b) color drilling images from the borehole

Listed in Table 4. According to the judgment of drilling imaging observation, the change of flushing fluid consumption and the change of water level during drilling, the vertex of the WCFZ was 242.5 m, the vertical depth of the roof from the hole mouth was 299.3 m at the location of borehole SW-02. Therefore, at the location of borehole SW-02, it was calculate based on Eq. 4 and Eq. 5 that the height of WCFZ and the height of caving zone were 53.92 m and 25.42 m.

Table 4 The height of the WCFZ in working face No. 12304

| Case mine | Working face | Borehole number | $M$ (m) | $H$ (m) | $H_k$ (m) | $H_{lie}$ (m) |
|---|---|---|---|---|---|---|
| Shangwan | 12304 | SD-SW-1 | 3.6 | 299 | 24.26 | 55.76 |
| | | SD-SW-2 | 3.6 | 299.3 | 25.26 | 53.76 |

# 5 Results and discussion

## *5.1 Correlation analysis of influence factors of the height of the WCFZ*

To further analyze the nature of each influencing factor, based on the grey incidence degree theories [31], the height of WCFZ was taken as the parent sequence, and the $L$, $M$, $H_d$, $D$, $V$, $b$ were taken as the sub sequence in Table 5. The value of correlation coefficient was calculated and shown in Table5. For the six evaluation items, the height of the WCFZ was significantly correlated with various influencing factors, and the degree of correlation was ranked as $L$, $V$, $M$, $b$, $H_d$, $D$, from high to low.

Table 5 Correlation coefficient between influencing factors and WCFZ

| Influencing factors | *L* | *M* | $H_d$ | *D* | *V* | *b* |
|---|---|---|---|---|---|---|
| Correlation coefficient | 0.770 | 0.718 | 0.681 | 0.623 | 0.736 | 0.713 |
| Ranking | 1 | 3 | 5 | 6 | 2 | 4 |

As listed in Table 6, the correlation matrix of the factors influencing the height of WCFZ was calculated using the Statistical Product and Service Solutions (SPSS) software. Previous studies have analyzed that the main influencing factors for the height of WCFZ were mining height and hard rock and were highly correlated [4,19]. This study shows that the *L*, *M*, $H_d$, *D*, *V* and *b* were positively correlated with the height of WCFZ, while the working face length and dip angle of coal seam were negatively correlated with the height of WCFZ. The mining depth, face advance speed and mining height were the main influencing factors on the WCFZ, while the proportion coefficient of hard rock was the indirect influence factor, as shown in Fig. 14. Therefore, the development of fracture zone was mainly influenced by three factors, which were the mining height, mining speed and length of working face in the Shendong mining area.

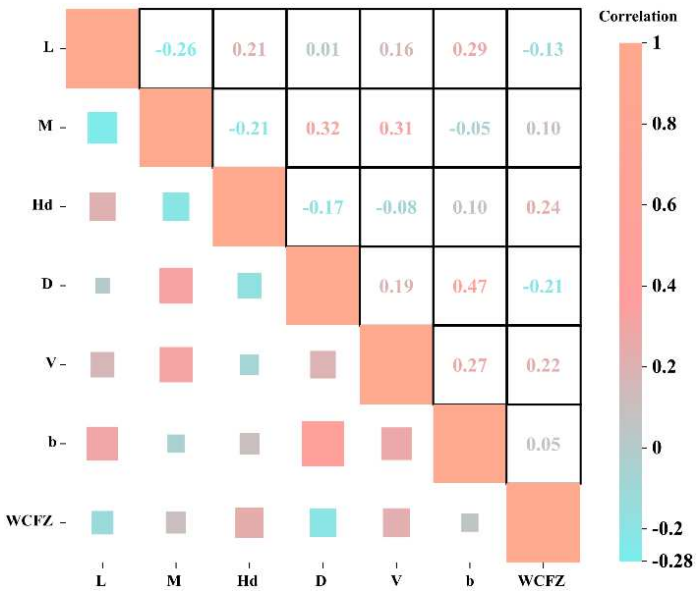


**Fig.14** Correlation heatmap of WCFZ and its influencing factors

Table 6 Correlation matrix between influencing factors and the WCFZ

| Influencing factors | *L* | *M* | $H_d$ | *D* | *V* | *b* | The height of WCFZ |
|---|---|---|---|---|---|---|---|
| *L* | 1 | | | | | | |
| *M* | -0.261 | 1 | | | | | |
| $H_d$ | 0.206 | -0.209 | 1 | | | | |
| *D* | 0.010 | 0.323 | -0.168 | 1 | | | |
| *V* | 0.161 | 0.314 | -0.082 | 0.193 | 1 | | |
| *b* | 0.291 | -0.052 | 0.098 | 0.475* | 0.274 | 1 | |
| The height of WCFZ | -0.129 | 0.102 | 0.240 | -0.206 | 0.217 | 0.048 | 1 |

Note: * mean significant correlation at P<0.05.

### *5.2 Comparative analysis of predicted values of WCFZ*

Table 7 shows that the field observations were very close to the forecast values of the GA-BP network model, indicating its practicality in Shendong mining area. The forecast values of the unoptimized BP network prediction model were larger compared with the field measured height of WCFZ. The analysis shows that the initial value of the un-optimized BP neural network with errors in the calculation process was not the optimal solution. Besides, the solution will be locally minimum and the

convergence rate was slow. The neural network may appear over fitting, which leads to low performance and poor fault tolerance [28,32]. However, the prediction error of GA-BP neural network was 7.78% and the error value was smaller than the error of empirical formula and BP neural network prediction model. Therefore, the trained GA-BP neural network prediction model can accurately predict the height of WCFZ in the Shendong mine area.

Table 7 The predicted value and observed value of WCFZ in the study area

| Method | Height of WCFZ（m） | Relative error |
|---|---|---|
| Observed value | 55.76 | — |
| Empirical formula 1: height of water-conducting fracture zone | 62.38 | 11.87% |
| BP neural network model | 69.7 | 25% |
| GA-BP neural network model | 60.10 | 7.78% |

## 6. Conclusion

By training the GA-BP neural network model, the height of WCFZ prediction value can be derived in Shendong mining area, and combined with the verification of engineering cases, the height of WCFZ can be accurately predicted in Shendong mining area. The main conclusions were as follows:

（1）The height of WCFZ was an indicator affected by multiple factors. The height of WCFZ was significantly correlated with various influencing factors, and the degree of correlation was ranked as $L$, $V$, $M$, $b$, $H_d$, $D$, from high to low. Therefore, the

development of fracture zone was mainly influenced by three factors, which were the mining height, mining speed and length of working face in the Shendong mining area.

（2）The training test with a typical mine working face as a sample was effectively verified, and a nonlinear prediction model of WCFZ height in the Shendong mine area was constructed. The model has high precision and general practicality for prediction of WCFZ height in Shendong mine area.

（3）Through the comparative analysis of different model calculations, the prediction error of BP neural network model was 11.87%, the error of empirical formula was 25%, while the prediction error of GA-BP model was 7.78%. Therefore, the height of WCFZ in the Shendong mine area can be effectively predicted using the trained GA-BP network model.

**Conflicts of Interest:** The authors declare that they have no conflict of interest.

## Acknowledgements

This work was supported by the Ordos Postdoctoral Research Fund (OPRF2403). The National Science Fund for Distinguished Young Scholars (No.52225402). These sources of supports are gratefully acknowledged.

## References

[1] Zhang H, Zhang J, Xu ZH, Zhang JW, Du SL, Wei SR, et al. Overburden breakage and surface damage evolution under high-intensity mining of shallow coal seams: evidence from Shendong mining area. Sci Rep 2025;15. https://doi.org/10.1038/s41598-025-05177-9.

[2] He X, Zhao YX, Zhang C, Han PH. A Model to Estimate the Height of the

Water-conducting Fracture Zone for Longwall Panels in Western China. MINE WATER Environ 2020;39:823–38. https://doi.org/10.1007/s10230-020-00726-2.

[3] Du Q, Guo GL, Li HZ, Sun JC, Hu ZQ. Overlying strata movement characteristics and water conducting fracture zone height prediction for deep coal mining in arid Western China. Sci Rep 2026;16. https://doi.org/10.1038/s41598-026-46768-4.

[4] He X, Zhao Y, Zhang C, Han P. A Model to Estimate the Height of the Water-conducting Fracture Zone for Longwall Panels in Western China. Mine Water Environ 2020;39:823–38. https://doi.org/10.1007/s10230-020-00726-2.

[5] Guo W, Zhao G, Lou G, Wang S. A New Method of Predicting the Height of the Fractured Water-Conducting Zone Due to High-Intensity Longwall Coal Mining in China. Rock Mech Rock Eng 2019;52:2789–802. https://doi.org/10.1007/s00603-018-1567-1.

[6] Xu D, Peng S, Xiang S, He Y. A novel caving model of overburden strata movement induced by coal mining. Energies 2017;10:1–13. https://doi.org/10.3390/en10040476.

[7] Liu Y, Tao L, Jiang L. Height of water-conducting fractured zone in coal mining in the soil – rock composite structure overburdens. Environ Earth Sci 2019;78:1–13. https://doi.org/10.1007/s12665-019-8239-7.

[8] Palchik V. Formation of fractured zones in overburden due to longwall mining. Environ Geol 2003;44:28–38. https://doi.org/10.1007/s00254-002-0732-7.

[9] Wang F, Xu J, Chen S, Ren M. Method to Predict the Height of the Water Conducting Fractured Zone Based on Bearing Structures in the Overlying Strata. Mine Water Environ 2019;38:767–79. https://doi.org/10.1007/s10230-019-00638-w.

[10]Fan H, Wang L, Lu Y, Li Z, Li W, Wang K. Height of water-conducting

fractured zone in a coal seam overlain by thin bedrock and thick clay layer: a case study from the Sanyuan coal mine in North China. Environ Earth Sci 2020;79:1–11. https://doi.org/10.1007/s12665-020-8873-0.

[11]Zhang D, Fan G, Ma L, Wang X. Aquifer protection during longwall mining of shallow coal seams: A case study in the Shendong Coalfield of China. Int J Coal Geol 2011;86:190–6. https://doi.org/10.1016/j.coal.2011.01.006.

[12]Yan W, Dai H, Chen J. Surface crack and sand inrush disaster induced by high-strength mining: example from the Shendong coal field, China. Geosci J 2018;22:347–57. https://doi.org/10.1007/s12303-017-0031-7.

[13]Miao X, Cui X, Wang J, Xu J. The height of fractured water-conducting zone in undermined rock strata. Eng Geol 2011;120:32–9. https://doi.org/10.1016/j.enggeo.2011.03.009.

[14]Liu X, Tan Y, Ning J, Tian C, Wang J. The Height of Water-Conducting Fractured Zones in Longwall Mining of Shallow Coal Seams. Geotech Geol Eng 2015;33:693–700. https://doi.org/10.1007/s10706-015-9851-2.

[15]Wang G, Wu M, Wang R, Xu H, Song X. Height of the mining-induced fractured zone above a coal face. Eng Geol 2017;216:140–52. https://doi.org/10.1016/j.enggeo.2016.11.024.

[16]Chen Y, Zhu S. Determination of caved and water-conducting fractured zones of “two soft and one hard” unstable coal seam. Acta Geod Geophys 2020;55:451–75. https://doi.org/10.1007/s40328-020-00300-w.

[17]Ren S, Cui F, Zhao S, Cao J, Bai J, Jiang Z, et al. Investigation of the Height of Fractured Water-Conducting Zone: A Case Study. Geotech Geol Eng 2021;39:3019–31. https://doi.org/10.1007/s10706-020-01675-x.

[18]Guo C, Yang Z, Li S, Lou J. Predicting the water-conducting fracture zone (Wcfz)

height using an mpga-svr approach. Sustain 2020;12:1–15. https://doi.org/10.3390/su12051809.

[19] Yang P, Yang W, Nie Y, Saleem F, Lu F, Ma R, et al. Predicting the Height of the Water-conducting Fractured Zone Based on a Multiple Regression Model and Information Entropy in the Northern Ordos Basin, China. Mine Water Environ 2022;41:225–36. https://doi.org/10.1007/s10230-021-00805-y.

[20] Tang M, Zhou C, Zhang N, Liu C, Pan J, Cao S. Prediction of the Ash Content of Flotation Concentrate Based on Froth Image Processing and BP Neural Network Modeling. Int J Coal Prep Util 2021;41:191–202. https://doi.org/10.1080/19392699.2018.1458716.

[21] Zhang Y, Cao S, Gao R, Guo S, Lan L. Prediction of the heights of the water-conducting fracture zone in the overlying strata of shortwall block mining beneath aquifers in western China. Sustain 2018;10. https://doi.org/10.3390/su10051636.

[22] Bi Y, Wu J, Zhai X, Huang K. A prediction model for the height of the water-conducting fractured zone in the roof of coal mines based on factor analysis and RBF neural network. Arab J Geosci 2022;15. https://doi.org/10.1007/s12517-022-09523-3.

[23] Liu M, Shi J. A cellular automata traffic flow model combined with a BP neural network based microscopic lane changing decision model. J Intell Transp Syst Technol Planning, Oper 2019;23:309–18. https://doi.org/10.1080/15472450.2018.1462176.

[24] Wang W, Tang R, Li C, Liu P, Luo L. A BP neural network model optimized by Mind Evolutionary Algorithm for predicting the ocean wave heights. Ocean Eng 2018;162:98–107. https://doi.org/10.1016/j.oceaneng.2018.04.039.

[25] Yang Y, Lai X, Luo T, Yuan K, Cui F. Study on the viscoelastic-viscoplastic model of layered siltstone using creep test and RBF neural network. Open Geosci 2021;13:72–84. https://doi.org/10.1515/geo-2020-0224.

[26] Hu Y, Li W, Liu S, Wang Q. Prediction of Floor Failure Depth in Deep Coal Mines by Regression Analysis of the Multi-factor Influence Index. Mine Water Environ 2021;40:497–509. https://doi.org/10.1007/s10230-021-00769-z.

[27] Hu W, Zhao C. Evolution of Water Hazard Control Technology in China's Coal Mines. Mine Water Environ 2021;40:334–44. https://doi.org/10.1007/s10230-020-00744-0.

[28] Lin H, Chen Z, Wu L, Lin P, Cheng S. On-line monitoring and fault diagnosis of PV array based on BP neural network optimized by genetic algorithm. Lect Notes Comput Sci (Including Subser Lect Notes Artif Intell Lect Notes Bioinformatics) 2015;9426:102–12. https://doi.org/10.1007/978-3-319-26181-2_10.

[29] Metawa N, Hassan MK, Elhoseny M. Genetic algorithm based model for optimizing bank lending decisions. Expert Syst Appl 2017;80:75–82. https://doi.org/10.1016/j.eswa.2017.03.021.

[30] Li JJ, He ZH, Piao CD, Chi WQ, Lu Y, Frappart F, et al. Research on Subsidence Prediction Method of Water-Conducting Fracture Zone of Overlying Strata in Coal Mine Based on Grey Theory Model. WATER 2023;15. https://doi.org/10.3390/w15234177.

[31] Feng JY, Shi XM, Chen JS, Wang K. Prediction of the Water-Conducting Fracture Zone Height Across the Entire Mining Area Based on the Multiple Nonlinear Coordinated Regression Model. WATER 2025;17. https://doi.org/10.3390/w17091303.

[32] Tan X, Ji Z, Zhang Y. Non-invasive continuous blood pressure measurement

520 based on mean impact value method, BP neural network, and genetic algorithm.
521 Technol Heal Care 2018;26:S87–101. https://doi.org/10.3233/THC-174568.
522